BBA - Biomembranes 1861 (2019) 1546–1557

Contents lists available at ScienceDirect

BBA - Biomembranes

journal homepage: www.elsevier.com/locate/bbamem

Heterologous expression of the mammalian sodium-nucleobase transporter rSNBT1 in *Leishmania tarentolae*

Anargyros Doukas[a], Ekaterini Karena[c], Maria Botou[c], Konstantinos Papakostas[c,1], Amalia Papadaki[a], Olympia Tziouvara[a], Evaggelia Xingi[b], Stathis Frillingos[c,*], Haralabia Boleti[a,b,**]

[a] Intracellular Parasitism Group, Microbiology Department, Hellenic Pasteur Institute, Vas. Sofias 127, Athens 11521, Greece
[b] Light Microscopy Unit, Hellenic Pasteur Institute, Vas. Sofias 127, Athens 11521, Greece
[c] Laboratory of Biological Chemistry, Department of Medicine, University of Ioannina, Greece

ARTICLE INFO

Keywords:
Leishmania tarentolae
Multispanning membrane protein expression
NAT/NCS2 family
rSNBT1 purine-pyrimidine permease

ABSTRACT

Recombinant expression systems for mammalian membrane transport proteins are often limited by insufficient yields to support structural studies, inadequate post-translational processing and problems related with improper membrane targeting or cytotoxicity. Use of alternative expression systems and optimization of expression/purification protocols are constantly needed. In this work, we explore the applicability of the laboratory strain LEXSY of the ancient eukaryotic microorganism *Leishmania tarentolae* as a new expression system for mammalian nucleobase permeases of the NAT/NCS2 (Nucleobase-Ascorbate Transporter/Nucleobase-Cation Symporter-2) family. We achieved the heterologous expression of the purine-pyrimidine permease rSNBT1 from *Rattus norvegicus* (tagged at C-terminus with a red fluorescent protein), as confirmed by confocal microscopy and biochemical analysis of the subcellular fractions enriched in membrane proteins. The cDNA of rSNBT1 has been subcloned in a pLEXSY-*sat-mrfp1*vector and used to generate transgenic *L. tarentolae-rsnbt1-mrfp1* strains carrying the pLEXSY-sat-*rsnbt1-mrfp1* plasmid either episomally or integrated in the chromosomal DNA. The chimeric transporter rSNBT1-mRFP1 is targeted to the ER and the plasma membrane of the *L. tarentolae* promastigotes. The transgenic strains are capable of transporting nucleobases that are substrates of rSNBT1 but also of the endogenous *L. tarentolae* nucleoside/nucleobase transporters. A dipyridamole-resistant Na^+-dependent fraction of uptake is attributed to the exogenously expressed rSNBT1.

1. Introduction

Membrane transport proteins represent about 5% of the total number of protein-coding genes in mammalian genomes and are essential in various aspects of human physiology and drug development. Despite their importance, membrane transporters and, in particular, solute carriers (facilitative and secondary active transporters) remain relatively understudied to date [1]. Among other technical challenges, one major bottleneck is the production of sufficient amounts of correctly folded and properly targeted recombinant proteins for subsequent structural-functional studies. As with mammalian membrane proteins in general, several cell host systems have been used to this end, including yeasts, the baculovirus-insect cell system and mammalian cell lines [2,3]. The applicability of these hosts may be subject to various limitations depending on the system [1] and unicellular hosts that are freed from disadvantages of low yield, slow growth and/or high cost of complex media often display problems in providing the proper membrane environment or effecting post-translational modifications for correct membrane insertion, folding and function of the heterologously expressed protein. In the present work, we explore an alternative unicellular host, the protozoan *Leishmania tarentolae* [4], as an expression system for mammalian membrane transporters.

Abbreviations: NAT, Nucleobase-Ascorbate Transporter; NCS2, Nucleobase-Cation Symporter-2; ENT, Equilibrative Nucleoside Transporter; Ab, antibody; mAb, monoclonal antibody; pAb, polyclonal antibody; FL, fluorescence; EP, episomal; CH, chromosomal; FL, Fluorescence; ER, Endoplasmic Reticulum; RT, Room Temperature

* Correspondence to: S. Frillingos, Laboratory of Biological Chemistry, Department of Medicine, University of Ioannina, Ioannina, Greece.
** Correspondence to: H. Boleti, Intracellular Parasitism group, Department of Microbiology and Light Microscopy Unit, Hellenic Pasteur Institute, Athens, Greece.
E-mail addresses: efriligo@uoi.gr (S. Frillingos), hboleti@pasteur.gr (H. Boleti).
[1] Current address: CeMM Research Center for Molecular Medicine of the Austrian Academy of Sciences, Vienna, Austria.

https://doi.org/10.1016/j.bbamem.2019.07.001
Received 19 March 2019; Received in revised form 26 June 2019; Accepted 2 July 2019
Available online 05 July 2019
0005-2736/

Leishmania tarentolae (*L. tarentolae*) is an ancient eukaryotic organism belonging to the *Leishmania* subgenus Sauroleishmania originally isolated from the gecko *Tarentola mauritanica* [5]. Although most species of the genus *Leishmania* are pathogenic to mammals, *Sauroleishmania* represents a lineage that switched from mammals to reptiles as their main hosts [6]. *L. tarentolae* lacks genes associated to the intracellular stage of human pathogenic species [7] and is known to parasitize only reptiles.

The laboratory strain *L. tarentolae* LEXSY, which is cultured in biosafety S1 conditions, has been used as an expression system for recombinant eukaryotic proteins because it offers a number of advantages over other unicellular hosts [4,8,9]. It has simple nutritional requirements in cell culture, it can be grown in large-volume cultures with a cell cycle of 6–10 h, the generation of transgenic promastigotes (the flagellated, extracellular form of *Leishmania*) is simple and easy with a stable cell line generated in 14–30 days and it can be grown in affordable nutrients like yeast extract to a very dense culture of up to 1×10^9 cells per mL. Importantly, the *L. tarentolae* LEXSY post-translational machinery is equipped with enzymes that carry out the *N*-glycosylation pattern of mammalian proteins with double antenna glycans, a property that is absent in yeast or insect hosts [9–11]. It also displays physical auxotrophy to several amino acids, a property that facilitates isotopic labeling of recombinant proteins for structural analysis [12,13]. *L. tarentolae* LEXSY had not been used for expression of eukaryotic membrane proteins until recently [14–16] and has not been applied to date for expression of mammalian secondary active transporters.

Herein, we explore *L. tarentolae* LEXSY as a recombinant expression host for the Na^+-nucleobase transporter rSNBT1 from *Rattus norvegicus* [17], a paradigm for mammalian permeases of the evolutionarily ubiquitous family NAT/NCS2 (Nucleobase-Ascorbate Transporter/Nucleobase-Cation Symporter-2) (Supplemental Fig. S1). This protein family belongs to the APC superfamily of secondary active transporters [18,19] and represents a distinct, recently described structural/mechanistic pattern that is shared by another two APC families [20–27]. It includes ion-gradient driven transporters of key metabolites or antimetabolite analogs with diverse substrate profiles, ranging from purine/pyrimidine permeases in bacteria, fungi, plants and metazoa to ascorbate (vitamin C) permeases in human and other mammals [28–36].

The mammalian NAT/NCS2 permeases constitute solute carrier family SLC23. Functionally known members include the human, rat and murine Na^+-ascorbate symporters SVCT1 and SVCT2 and the rat Na^+-uracil/purine symporter rSNBT1. There are no structural studies available for these homologs and studies on the functional role of key amino acid residues are limited for SVCT1/2 [29,37,38] and lacking for rSNBT1. The rat intestinal rSNBT1 is the first mammalian (or metazoan) permease to be recognized to transport nucleobases as major substrates, whereas its putative human ortholog (*slc23a4*) has been evolutionarily inactivated and remains as a pseudogene [17]. Despite the difference in substrates, rSNBT1 is closely related in sequence (> 50% identity, > 70% similarity) with SVCT1/2. Interestingly, previous work using mammalian cell cultures has identified that *N*-glycosylation is required for membrane targeting and functionality of hSVCT1 or hSVCT2 [39,40].

We now use the *L. tarentolae* LEXSY system for expression of the rSNBT1 in recombinant form and demonstrate that recombinant rSNBT1 is targeted to the ER and the plasma membrane of *L. tarentolae* promastigotes.

2. Materials and methods

2.1. Reagents, radiochemicals and antibodies

All chemicals used were of analytical grade and obtained from commercial sources, unless otherwise stated. The cDNA of rSNBT1 (cloned in the pCI-neo mammalian expression vector) was a generous gift of Dr. Hiroaki Yuasa, Nagoya City University, Japan. Enzymes and DNA molecular mass standards were purchased from Roche (New England Biolabs) and KAPA Biosystems. Protein molecular mass standards were purchased from Amersham Biosciences. The anti-α-Tubulin (T5168) mouse monoclonal antibody (mAb) was from Sigma. The BiP/GRP78 rabbit polyclonal antibody (pAb) specific for Trypanosomatid parasites was a kind gift of Dr. J. D. Bangs, University at Buffalo (SUNY). The anti-mRFP antibody was prepared as described previously [41]. Fluorochrome-conjugated secondary antibodies (Alexa Fluor® 546 and Alexa Fluor® 488 conjugated to anti-rabbit or anti-mouse Abs) were from Molecular Probes. The radiolabeled nucleobases used in the transport assays, namely [5,6-^{3}H]-uracil (40 Ci mmol^{-1}), [8-^{3}H]-xanthine (22.8 Ci mmol^{-1}), [2,8-^{3}H]-hypoxanthine (27.7 Ci mmol^{-1}) and [2-^{14}C]-thymine (57 mCi mmol^{-1}), were obtained from Moravek Biochemicals (Brea, CA). Non-radiolabeled nucleobases or analogs were from Sigma-Aldrich (St. Louis, MO).

2.2. Cell culture

Leishmania tarentolae promastigotes (LEXSY strain, Jena Bioscience) were cultured at 25°C, in Brain Heart Infusion (LEXSY Broth BHI) medium supplemented with Hemin (Bovine Hemin Chloride, Sigma) at a final concentration of 0.25% (w/v), 10 μM L-biopterin (Cayman), 1 unit/ml penicillin (Sigma) and 0.1 mg/ml streptomycin.

2.3. Plasmid construction

The cDNA of *rsnbt1* from *Rattus norvegicus* (AB511909.1, translated sequence: GenBank: BAI66650.1) was transferred to the pLEXSY-sat-*mrfp1*plasmid [41] by PCR and restriction fragment insertion. The *rsnbt1* cDNA was amplified from pCI-neo-*rsnbt1* [17] using the primers 5′-GCTAGCAGATCTCCATGAACTCTGCAGTCTGC-3′ and 5′-CGCAGCAGATCTCATCTTGGTCTCTGTAACACTCC-3′, engineered to contain a *Bgl*II recognition site (underlined) for insertion into the *Bgl*II site of pLEXSY-sat-*mrfp1*. To ensure the correct orientation and in-frame insertion of the PCR product (*rsnbt1* cDNA), the ligation products were used to transform *Escherichia coli* Top10F′ (Invitrogen), recombinant clones were selected on Luria-Bertani (LB) agar containing ampicillin (0.1 mg/mL), plasmid DNA from the resulting clones were screened for presence of the correct-size insert with restriction analysis and finally, two of the insert-positive clones were verified by double-strand DNA sequencing through the ligation junctions (Eurofins Genomics GmbH). Both clones had the *rsnbt1* cDNA insert at the correct orientation and frame.

2.4. Generation of L. tarentolae transgenic promastigotes

For episomal expression, *L. tarentolae* parasites were transfected with pLEXSY-sat-*rsnbt1-mrfp1*plasmid by electroporation. For integration of the *rsnbt1-mrfp1* gene into the *L. tarentolae* chromosomal DNA (*ssu* locus of the small ribosomal subunit), the pLEXSY-sat-*rsnbt1-mrfp1* plasmid was digested with *Swa*I, a ~7200 bp restriction fragment containing the transgene and the *sat* marker for antibiotic resistance was purified from agarose gel and was used to transfect *L.tarentolae* promastigotes at the logarithmic phase of growth by electroporation, according to a previously described protocol [41].

Selection of the transgenic population was performed by culturing the electroporated parasites at 25 °C in BHI medium containing the antibiotic nourseothricin (Jena Bioscience). Nourseothricin was added initially at a concentration of 10 μg/ml 24 h after electroporation and then, sequentially, at two-fold higher concentration every 3–4 days in culture, up to a final concentration of 100 μg/mL. Selection of the recombinant LEXSY clones on the basis of nourseothricin resistance was allowed by the *sat* marker gene (encoding streptothricin acetyltransferase) [4].

2.5. Detergent-based fractionation

Digitonin (Sigma) fractionation of L. *tarentolae-rsbt1-mrfp1* ($\sim 2 \times 10^9$ cells, enumerated by the use of a Mallassez cytometer or by measuring turbidity of the cell suspension at OD_{600nm}) was performed as described previously for other *Leishmania* species, according to an established protocol [41,42]. Briefly, cells were treated initially with 20 μM digitonin and the soluble product (supernatant) was recovered after centrifugation at 18,000*g* for 5 min (fraction F1). The pellet was further treated with 200 μM digitonin and the new supernatant was recovered as fraction F2 while the pellet was treated with 1 mM digitonin. The supernatant from the third step, (fraction F3) was recovered and the pellet was treated with 10 mM digitonin to give a soluble product (fraction F4) and a pellet (fraction F5) collected after centrifugation in the fourth step. Fraction 5 was further solubilized with 2% (v/v) Triton X-100 (1 h, 4 °C) and the soluble (F5 S) and insoluble (F5 P) fractions were recovered by centrifugation (20,000 *g*, 20 min, 4 °C). The protein fractions F1–F4 were obtained after acetone precipitation (overnight, −20 °C).

2.6. Protein electrophoresis and Western blot

Proteins, solubilized in Laemmli sample buffer after incubation at 25°C for 1 h, were separated by SDS-PAGE (10% gel; [43]) and transferred to Hybond-C nitrocellulose (Amersham) using a wet blotting apparatus (Biorad). The membranes were blocked overnight at 4 °C and then treated with the anti-mRFP pAb (0.4 μg/ml), as previously described [41]. After several washes in Tris-buffered saline containing 0.1% (v/v) Tween 20, the blots were incubated (1 h, RT) with HRP-labeled anti-rabbit Ab diluted to 1:1000 (Amersham). Signals were developed by enhanced chemiluminescence (ECL plus system, Amersham). Blots were either analyzed in a Phosphoimager or exposed to Kodak photographic films further developed with Kodak reagents. The ImageJ software [44] was used to quantify the signal on the digital images of the film.

2.7. Immunofluorescence and quantitative confocal microscopy

L. tarentolae promastigotes were fixed, allowed to attach on poly-L-lysine coated coverslips and labeled with primary and secondary antibodies, as previously described [41]. *L. tarentolae* stationary phase promastigotes expressing the rSBT1-mRFP1 immobilized on poly-lysine coated coverslips were fixed with paraformaldehyde [4% (w/v) in PBS], and either mounted directly on microscope slides or further stained with either the α-tubulin mAb (dilution 1:300) or the BiP/GRP78 [45] pAb (dilution 1:500) followed by the anti-mouse or anti-rabbit pAbs conjugated to Alexa Fluor® 488 before mounting with Mowiol [10% (w/v) Mowiol 4–88 (Calbiochem), 25% (v/v) glycerol, 100 mM Tris/HCl, pH 8.5] on microscope slides, sealed with nail polish and stored at 4 °C. Microscopic analysis of the samples was performed in a Leica TCS SP or SP8 confocal microscopes using the 63X lens. Red fluorescence (FL) was acquired with the Argon laser 543 nm line (TCS-SP) or the Solid state laser 552 nm line (TCS-SP8P).

The percentages of transgenic red fluorescent parasites in each strain and the mean intensity FL/cell were calculated by assessing 8 fields per case with a total of 100–150 cells. Cell counting and red FL intensity levels (mRFP1 FL) was performed in maximum projections of 5 optical sections (0.5 μm step size)/field with the icy algorithm (see below) applying the Intensity Projection and HK-means tools.

The extent of colocalization between the tubulin of the *Leishmania* subpellicular microtubules and the rSNBT1-mRFP or monomeric mRFP (green and red FL respectively) was measured using the 3D "Coloc" module of Imaris v8.3.1, which utilizes the algorithms introduced by Costes et al. for the automatic selection of thresholds of the image channels [46]. We have used a third channel as a masking area for the entire analysis (created with the channel Arithmetic function "sqrt (ch1*ch2)", to exclude the background pixels of the dataset from the colocalization analysis. The mask channel is used in conjunction with the automatic threshold function. In this way, Imaris Coloc generates a new channel (the colocalization channel), which only contains voxels that represent the colocalization between the red and green channels. The thresholded Mander's coefficients were taken into account and threshold 10 was used for the analysis of the data.

2.8. Nucleobase uptake assays

L. tarentolae (LEXSY) and transgenic *L. tarentolae-rsnbt1-mrfp1*–CH (carrying the *rsnbt1-mrfp1* transgene integrated into the chromosomal DNA) or *L. tarentolae-mrfp1* (*mrfp1*) promastigotes were grown in LEXSY Broth BHI with appropriate supplements, in the presence of nourseothricin (1 μg/ml). Logarithmically grown cells were harvested (at an OD_{600nm} of 1.0 corresponding approximately to 10^8 cells/ml), washed twice in uptake buffer (Hepes 10 mM, pH 7.5, containing NaCl 140 mM, KCl 5 mM, KH_2PO_4 0.4 mM, $CaCl_2$ 1 mM, $MgSO_4$ 0.8 mM and glucose, 25 mM), normalized to an OD_{600nm} of 5.0 in the same buffer, and 50×10^6 cells per reaction were assayed for active transport of [^{3}H]-uracil (0.02, 0.05, 0.1, 0.2, 0.5 and 1 μM), [^{3}H]-xanthine (1 μM), [^{3}H]-hypoxanthine (1 μM) or [^{14}C]-thymine (10 μM). Transport assays were performed at 25 °C. After termination of reactions, samples were rapidly filtered through Whatman GF/C (1.2-μm borosilicate glass microfiber) filters, washed twice immediately with 3 mL of ice-cold KL buffer (KP_i, 0.1 M, pH 5.5, LiCl, 0.1 M) and taken for liquid scintillation counting.

All time-course experiments showed a roughly linear accumulation of substrates within the first 5 min of reaction. To determine nucleobase uptake activities, transport rates were determined from measurements at 1, 2 and 5 min. For determination of substrate specificity properties or effects of inhibitors, some transport assays were performed in uptake buffer containing choline chloride instead of NaCl at equimolar concentration (140 mM), or in the presence of dipyridamole (Sigma-Aldrich) or non-radiolabeled nucleobases.

2.9. Bioinformatics and statistical analysis

Comparative analysis of NAT/NSC2 and ENT sequences was based on BLAST-p search (https://blast.ncbi.nlm.nih.gov/Blast.cgi) and multiple sequence alignment using MUSCLE (https://www.ebi.ac.uk/Tools/msa/muscle/). The phylogenetic tree shown in Fig. S1 was constructed and analyzed with MEGA7 [47]. The most recent genome annotations were used in all cases to retrieve sequence data. The data on *L. tarentolae* and other *Leishmania* species were retrieved from the Kinetoplastids Genomics Resource (http://tritrypdb.org/tritrypdb/) [48].

The icy computational algorithm (http://icy.bioimageanalysis.org/) was used for quantitative image analysis of the confocal microscopy images applying the Intensity Projection and HK-means tools. For the colocalization analysis we used the 3D "Coloc" module of Imaris v8.3.1. Statistical analysis was performed with the GraphPad Prism 5.0 version.

2.10. Protein structure modeling

The rSNBT1 sequence was threaded on the template of UraA 5XLS [27] or UapA 5I6C [20] using the SWISS-MODEL server [49] and the modeled structures were visualized and analyzed with PyMOL (Schrödinger, LLC, New York, NY, USA).

3. Results and discussion

3.1. Cloning of the rsnbt1cDNA into the pLEXSY-sat-mrfp1Leishmania specific expression plasmid

The *rsnbt1*cDNA was cloned in the pLEXSY-sat-*mrfp1* expression

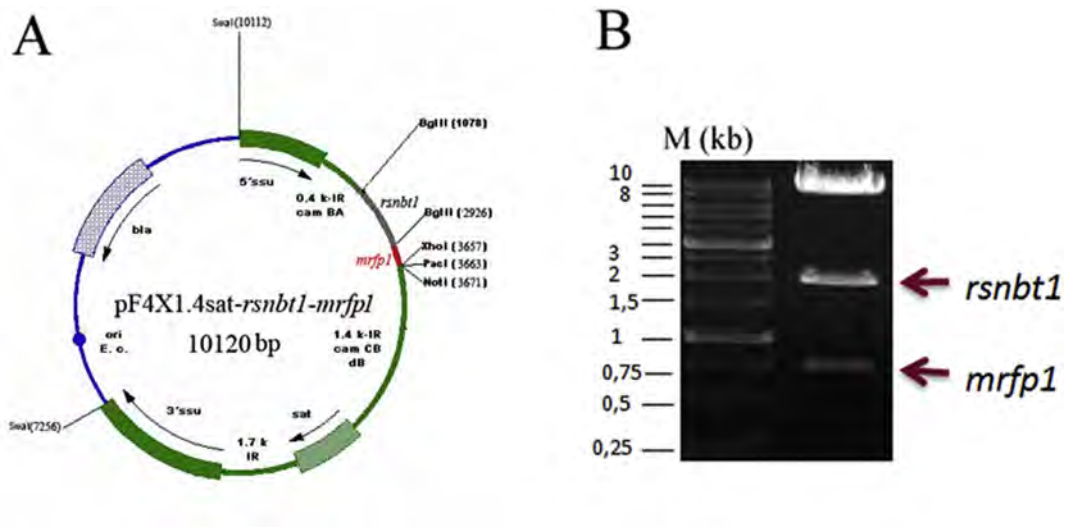

Fig. 1. Cloning of the rsnbt1 cDNA in the pLEXSY-sat Leishmania specific vector. A. Map of the constructed pLEXSY-sat-*rsnbt1-mrfp1* plasmid with the *rsnbt1* cDNA inserted in the *Bgl*II site in frame with the *mrfp1*gene between the *Bgl*II and *Xho*I sites. B. Analysis on agarose gel (1% w/v) of the RE reaction products of a positive pLEXSY-sat-*rsnbt1-mrfp1*clone after digestion with *Bgl*II and *Xho*I.

vector in frame with the gene coding for the red fluorescent protein mRFP1 to generate the pLEXSY-sat-*rsnbt1-mrfp1* recombinant plasmid (Fig. 1A), as described in *Materials andMethods*. Insertion of the correct size PCR product (1842 bp; corresponding to the full-length cDNA of *rsnbt1*) and correct orientation of the insert was verified by restriction with *Bgl*II and *Xho*I (Fig. 1B) and by double-strand DNA sequencing.

3.2. Generation of transgenic L. tarentolae-rsnbt1-mrfp1strains

The pLEXSY-sat-*rsnbt1-mrfp1*plasmid was used to generate transgenic parasites *L. tarentolae* that would express the chimeric rSNBT1-mRFP1 protein. Logarithmically growing *L. tarentolae* promastigotes were electroporated with circular supercoiled plasmid, for generation of strains expressing the recombinant rSNBT1-mRFP1 episomally, or with a linear DNA fragment of ~7200 bp containing the *rsnbt1-mrfp1*(2532 bp) transgene and the *sat* marker for antibiotic resistance that had been generated by digestion with *Swa*I (Fig. 1A). This linear DNA fragment contains sequences for homologous recombination at the *ssu* locus of the small ribosomal subunit and is expected to be integrated in this specific chromosomal locus allowing the generation of stable transgenic*L. tarentolae* strains.

Selection of the transgenic *L.tarenolae-rsnbt1-mrfp1* populations (episomal or stable strains) was achieved by culturing the electroporated parasites on gradually increasing concentrations of nourseothricin (up to 100 μg/ml) at 25 °C as described in the *Materials and Methods* section (Section 2). Expression of the recombinant rSNBT1-mRFP1 protein was confirmed by fluorescence microscopy (monitoring the expression of the red fluorescent protein mRFP1) (Fig. 2). Recombinant populations expressing rSNBT1-mRFP1 episomally (EP) were designated *L.tarentolae-rsnbt1-mrfp1*-EP and recombinant populations expressing rSNBT1-mRFP1 after integration of the transgene in the host chromosome (CH) were designated *L. tarentolae-rsnbt1-mrfp1*-CH.

In both recombinant populations, the percentage of cells expressing rSNBT1-mRFP1 was quantified by counting the number of cells with red FL and the chimeric rSNBT1-mRFP1 expression levels were assessed by determining the mean FL intensity per cell (Fig. 2B).

The percentage of parasites with detected levels of red FL averaged 60–70% of the total population enumerated in the phase contrast images. Red FL in parasites transfected with the linear DNA piece containing the *rsnbt1-mrfp1* expression cassette and expected to have the transgene integrated in their chromosomes was detected in approximately 70% of the total *L. tarentolae-rsnbt1-mrfp1*-CH population, whereas in those expressing the chimeric transporter episomally, the population with red FL averaged at around 60% of the total *L. tarentolae-rsnbt1-mrfp1*-EP population (Fig. 2B, left panel). Quantification of the red FL intensity per parasite showed that the expression of the chimeric transporter in the stable parasite strain was ~4-fold higher as compared to that of the episomal expression (Fig. 2B, right panel). In conclusion, the expression level of the rSNBT1-mRFP1 protein was significantly higher in the population of transgenic parasites expected to express it stably.

The growth rates of the transgenic *L.tarentolae-rsnbt1-mrfp1* populations expressing the chimeric transporter episomally (EP) or chromosomally (CH), estimated from curves depicting growth of promastigote parasite cultures for a period of 4 days (Supplementary Fig. S2), did not show significant differences from the growth rates of the wild-type *L. tarentolae* parental line. The doubling time in the three strains during the logarithmic phase of growth was calculated to be approximately 10 h.

3.3. Subcellular localization and plasma membrane targeting of the recombinant rSNBT1-mRFP1 in the transgenic L. tarentolae-rsnbt1-mrfp1 promastigotes

The localization of the recombinant protein in the transgenic strains *L. tarentolae-rsnbt1-mrfp1* (EP or CH) was analyzed by confocal microscopy both at the logarithmic (data not shown) and at the stationary phase of growth (Fig. 3 and Supplemental Figs. S3, S4 and S5) of the promastigote cultures. The rSNBT1-mRFP1 was detected mainly in the cell body of the promastigotes. Low staining was observed in the flagella after quantitative image analysis using the Imaris 8.3.1 software (Fig. S5). More explicitly, mRFP1 FL was detected at the promastigote cell surface (Fig. 3A, Fig. S3 framed cell) in ER-like structures (Fig. 3C, Fig. S3), and at the flagellar pocket (Fig. 3A arrow, Fig. S3 arrowheads), as expected for surface membrane proteins.

To evaluate the plasma membrane and ER localization we performed indirect immunofluorescence staining with specific antibodies recognizing either the α-tubulin of the subpellicular microtubules beneath the surface membrane of the parasite (Figs. 3A, S4) or the BiP/GRP78 protein that localizes in the ER lumen of *Trypanosomatidae* [45] (Fig. 3C). The α-tubulin of the subpellicular microtubules was labeled with a specific monoclonal antibody. The subpellicular microtubules found in some protozoa are a special type of microtubule arrangement

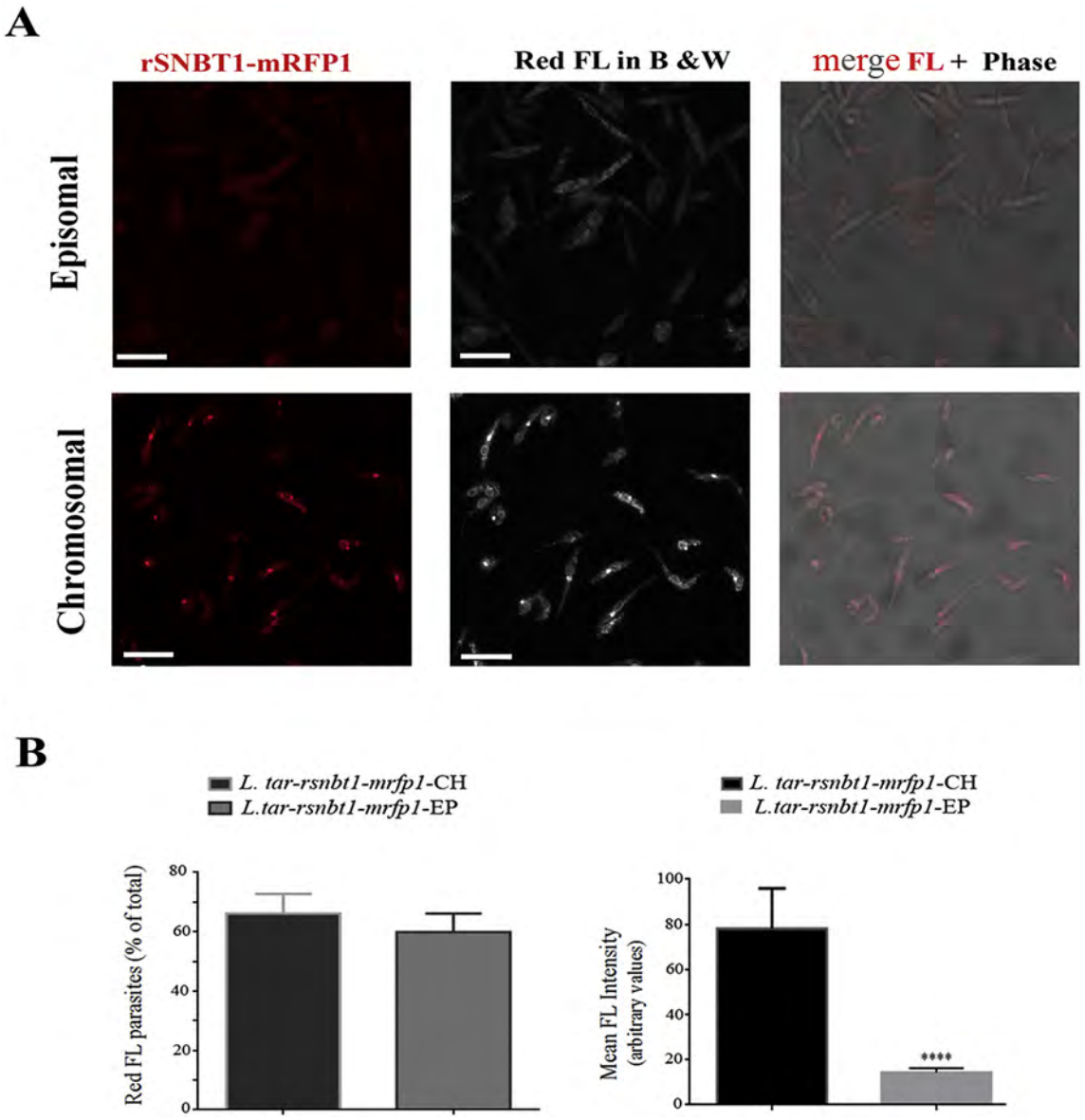

Fig. 2. Analysis of rSNBT1-mRFP1 expression in the trasngenic *L. tarentolae-rsnbt1-mrfp1* strains by microscopy. A. Confocal microscopy images of transgenic *L. tarentolae-rsnbt1-mrfp1* promastigotes at the late logarithmic phase of growth expressing episomally (*L. tarentolae-rsnbt1-mrfp1*-EP) or stably (*L. tarentolae-rsnbt1-mrfp1*-CH) the rSNBT1-mRFP1 protein. Red FL images were acquired with the Argon laser 543 nm using the Apochromat 63× lense and electronic image magnification 2×. Representative images selected randomly from fields with 1024 × 1024 pixel size are maximum projections of five optical sections acquired with a step size of 0.5 μm. The red FL of rSNBT1-mRFP1 is also shown in black and white in the center, for better contrast. Merged images of red FL and phase contrast at 60% transparency are shown on the right. All images were acquired in exactly the same laser intensity and photomultiplier (PMT gain) parameters. Scale bar: 8 μm. B. Graphical representation of the percentages of red fluorescent parasites in the transgenic strains (*L. tarentolae-rsnbt1-mrfp1*-EP and L. *tarentolae-rsnbt1-mrfp1*-CH) and of the mean mRFP FL intensity/cell in each strain quantified by the icy algorithm. Results are from 8 separate fields per case. A total of 100–150 parasites identified by the corresponding phase contrast images were analyzed in each case. Cell numbers and red FL intensity levels (mRFP1 FL) were determined at maximum projections of 5 optical sections (0.5 μm step size)/field by applying the Intensity Projection and HK-means tools of the icy algorithm. The t-paired test (GraphPad style of Prism 5.0) was used to compare the FL intensity in the two transgenic parasite populations ($p < 0.0001$, denoted with four asterisks on the gray bar, indicates significantly different values).

organized as a single layer immediately underneath the plasma membrane and in the trypanosomatids they are physically connected to the plasma membrane [50]. Profiles of the ER that radiate toward the periphery of the cell penetrating between the subpellicular microtubules and reaching the plasma membrane create the so-called cortical ER [51].

As shown in Fig. 3, red and green FL signals colocalize to a significant degree, indicating the presence of rSNBT1-mRFP1 in the plasma membrane or the ER of the transgenic parasites, as expected for a transmembrane transporter that is recognized by the protozoan secretory system of *L. tarentolae* for sorting and targeting to the plasma membrane. Consistently, the fluorescent chimeric transporter is detected also on the flagellar pocket (Fig. 3A, second row panels, arrow, and Fig. S3, arrowheads). The flagellar pocket is the main exocytic/endocytic domain of the *Leishmania* cell surface membrane where integral membrane proteins targeted to the parasite plasma membrane are concentrated before diffusing to the surface membrane [41,52].

Colocalization of rSNBT1-mRFP1 with α-tubulin was quantitated using the digital image analysis algorithm Imaris 8.3.1 coloc module. The protocol followed is described in *Materials andMethods*. As shown in Fig. 3B (left panel) in the bar graph of the thresholded Manders coefficients [46], the pixels with red FL (thresholded Manders coefficient B,

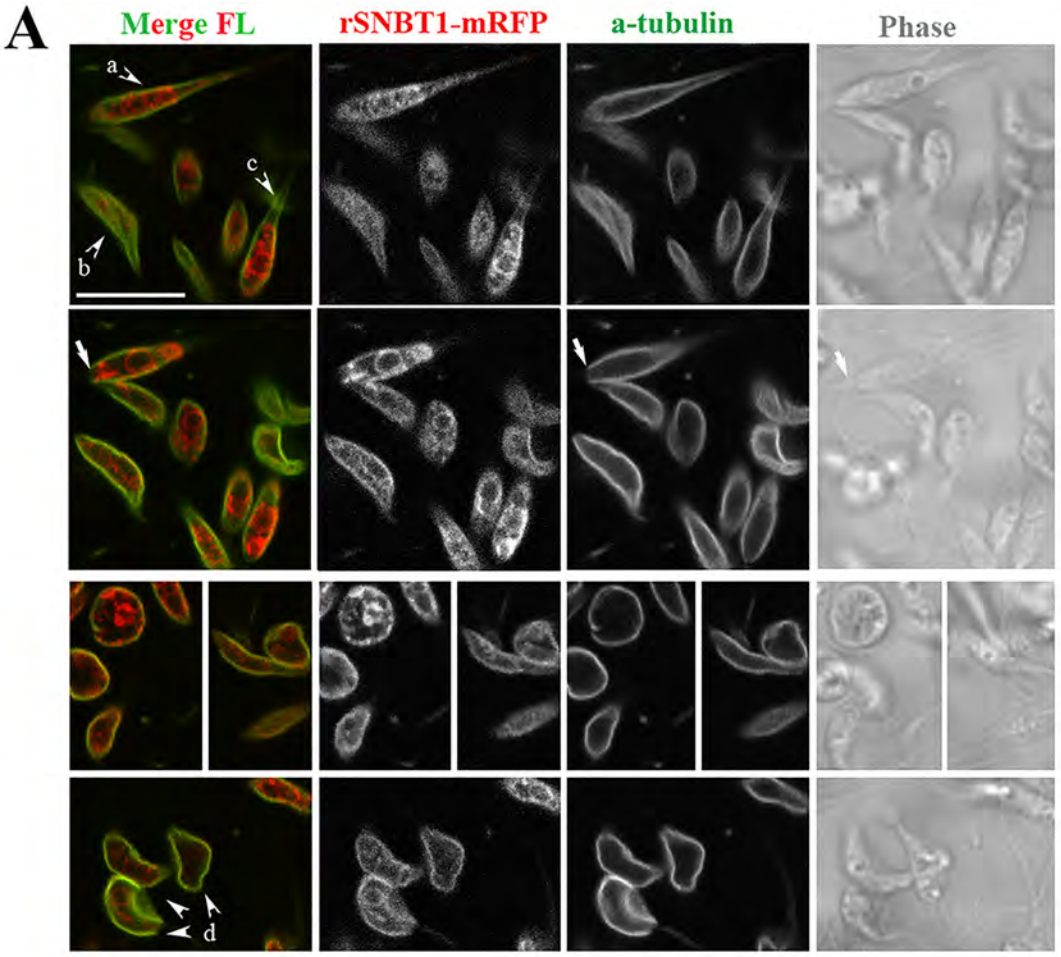

(caption on next page)

Fig. 3. Analysis of rSNBT1-mRFP1 localization in *L. tarentolae*-rsnbt1-mrfp1trangenic promastigotes by microscopy.A. Confocal microscopy images of *L. tarentolae-rsnbt1-mrfp1*-CH promastigotes at stationary phase of growth acquired with the TCS SP Leica microscope. Colocalization of the recombinant transporter rSNBT1-mRFP1 with α-tubulin of the subpellicular microtubules (A, B) or with the BiP/GRP78 ER chaperone (C) was detected by indirect immunofluorescence and confocal fluorescence microscopy imaging. Subpellicular microtubules were labeled with the anti-α-tubulin mAb (1:300) and the secondary anti-mouse pAb conjugated to Alexa Fluor 488. The BiP protein was stained with the anti-BiP rabbit pAb (serum dilution 1:500) and an anti-rabbit pAb conjugated to the Alexa Fluor 488. The red (mRFP1) and green (Alexa 488) FL are presented as black and white images in the central panels. Overlay of red and green FL is presented in color on the left (merge). (A) In four panels are presented cells from different singe optical sections of a z stack (7 images acquired at a step size of 0.5 μm) of the same imaged field (Fig. S4). The upper two panels are different optical sections of the same area. The arrow in the second upper panel indicates the flagellar pocket region. The round cell without flagellum (third series of panels), most probably represents a stressed cell. The irregular shapes observed for some promastigotes (fourth series of panels) may be due to folding of the promastigotes during attachment to the glass slide (see corresponding phase contrast images). C insets. Detail of the framed area magnified 2 X. Arrowheads in C show the beginning of the flagellum of the depicted promastigote. Corresponding phase contrast images are shown on the right. Scale bar: 8 μm. **(B)** Quantitative analysis of α-tubulin (green FL) and rSNBT1-mRFP1 or mRFP1 (red FL) colocalization. (Left) Plot of the mean (and SD values from 24 determinations) thresholded Manders coefficientA for green pixels overlapping with red pixels and the thresholded Mander's coefficient B for red pixels overlapping with green pixels in 3D. The values were derived by analyzing all cells of the field presented in Fig. S4 in all 7 optical sections of the depicted field (for rSNBT1-mRFP1) or from 33 cells from different fields including the ones presented in Fig. S6 (for mRFP1 control, derived from similarly treated *L. tarentolae-mrfp1* promastigotes) in all 9–13 optical sections, following the protocol described in Methods. (Right). 2D-Histogram plots of the colocalization analysis of the cells a, b, c and d shown by arrowheads in panels in A.

corresponding to the mRFP1 fluorescence) were found to colocalize at 68.08 ± 10.6% (n = 30 cells from one field) with the pixels with green FL (thresholded Manders coefficient A, corresponding to the α-tubulin staining). The high degree of colocalization of the red (rSNBT1-mRFP1) with the green FL (α-tubulin) is highlighted in the 2D histograms showing the correlation of the pixel intensities, over all pixels/voxels in the image, produced for four different cells (a, b, c) or cell clusters (d) (Fig. 3B, right panel), with a higher colocalization of the red with the green FL at the cell surface. The lower percentage of green pixels colocalizing with red pixels probably reflects the staining of the flagella where the red FL was very low (Fig. S5) as well as some background staining of soluble α-tubulin in the interior of promastigote cell.

An identical colocalization analysis was performed with *L. tarentolae-mrfp1* promastigotes expressing mRFP1 only, to estimate a baseline colocalization value for mRFP1 and tubulin (representing random colocalization). In these promastigotes, the mRFP1 fluorescence showed a diffuse cytosolic and nuclear distribution (Fig. S6), a pattern distinctly different from that observed for the localization of rSNBT1-mRFP1 (Fig. 3A), as expected for a soluble and a membrane-bound protein respectively. The pixels with red FL (thresholded Manders coefficient B, corresponding to the mRFP1 fluorescence) were found to colocalize at 17.30 ± 16.35% (n = 33 cells from different fields of view) with the pixels with green FL (thresholded Manders coefficient A, corresponding to the α-tubulin staining). Although there was a high degree of variability from cell to cell in this result, the above value could represent an approximation to a baseline random colocalization of soluble mRFP1 fluorescence with tubulin staining.

Subsequently, in order to quantify the amount of red FL at the cell surface and intracellularly, we applied another protocol of image processing and analysis using the Imaris 8.3.1. surface rendering tool. Using the 3D data of the imaged field presented in Fig. S4, we defined two surfaces, one for the “red channel” and one for the “green channel” (Fig. S5). We then calculated the “intensity sum” of the red channel. Subsequently, we created a “masked red channel”, which contains only the red voxels that are inside the “green surface”. A new surface for the “masked red channel” was created and from that we calculated an intensity sum corresponding to the fluorescence at the cell surface. Following this approach, we were able to calculate the intensity of red FL in 3D in all the cells in the imaged field depicted in Fig. S4 as well as the fluorescence that is localized at the surface of these cells, as defined by the red voxels that are inside the “green surface”. With this approximation we estimated that 41.85 ± 9.03% (result from analysis of 30 cells) of the total red FL is localized at the cell surface as defined by the staining of the subpellicular microtubules. Thus, it appears that a significant fraction of red FL, corresponding to rSNTB1-mRFP1, is localized at the promastigotes' cell surface, albeit with a significant variation depending on each cell. Admittedly, the resolution of confocal microscopy is not sufficient to distinguish between the plasma membrane-associated or cortical ER-associated rSNBT1-mRFP1 detected to colocalize with subpellicular microtubules. Therefore, it is not possible to quantitate the percentage of red FL (rSNBT1-mRFP1) colocalizing with green FL (subpellicular microtubules) at the *L. tarentolae* surface above the subpellicular microtubules (plasma membrane) or below them (cortical ER). However, the partial colocalization that we observed with the ER marker BiP (Fig. 3C) implies that a significant fraction of the red FL has to be attributed to plasma membrane-associated rSNBT1-mRFP1.

To estimate, again as an approximation, the amount of rSNBT1-mRFP1 colocalization with subpellicular microtubules that could correspond to random colocalization of free mRFP1 or soluble proteolytic fragments of the recombinant transporter tagged with mRFP1 localizing under and/or close to the subpellicular microtubules, we performed in the imaged *L. tarentolae-mrfp1* promastigotes a similar quantitative analysis as for the*L. tarentolae-rsnbt1-mrfp1* promastigotes using the Imaris 8.3.1 surface rendering tool. Cumulative quantitative results from analyzing 40 cells from different fields (including the ones presented in Fig. S6) with representative levels of mRFP1 and tubulin staining showed that 25.97 ± 8.94% of the total red fluorescence localized at the cell surface as defined by the staining of the subpellicular microtubules. This result implies that the percentage of red FL estimated to localize at the surface of the *L. tarentolae-rsnbt1-mrfp1* promastigotes (41.85 ± 9.03%) is actually attributed to rSNBT1-mRFP1 only in part, the actual contribution of rSNBT1-mRFP1 being probably at the range of about 16%. Of course, the two cell populations are not directly comparable, because the level of FL intensity due to soluble mRFP1 in the *L. tarentolae-rsnbt1-mrfp1* promastigotes is not the same as in the *L. tarentolae-mrfp1* promastigotes (Figs. 3A, S6).

The subcellular localization of the rSNBT1-mRFP1 protein was verified biochemically, by western blot analysis, in protein fractions from *L.tarentolae-rsnbt1-mrfp1*-CH promastigotes enriched in ER and plasma membrane proteins. Biochemical subcellular fractionation was achieved by treatment of the *L. tarentolae* promastigotes with gradually increasing concentrations of digitonin (20 μM to 10 mM) [42]. This fractionation procedure leads to a collection of five fractions with varying protein composition. Fractions F1 and F2 contain mainly soluble cytoplasmic proteins, F3 and F4 contain soluble and membrane proteins from intracellular organelles including the endoplasmic reticulum [41,42]. The final insoluble fraction 5 (F5), enriched in plasma membrane proteins, cytoskeleton and nuclear proteins [42], was further treated with 2% v/v Triton X-100 for one hour at 4 °C. After this treatment, F5 was subjected to an additional centrifugation step yielding a soluble fraction enriched in plasma membrane proteins (supernatant; designated F5s) and an insoluble pellet containing cytoskeleton and nuclear proteins (insoluble pellet; designated F5in). The rSNBT1-mRFP1 protein was detected with the anti-mRFP pAb as a single band with an apparent molecular mass of ~ 95 kDa, close to its

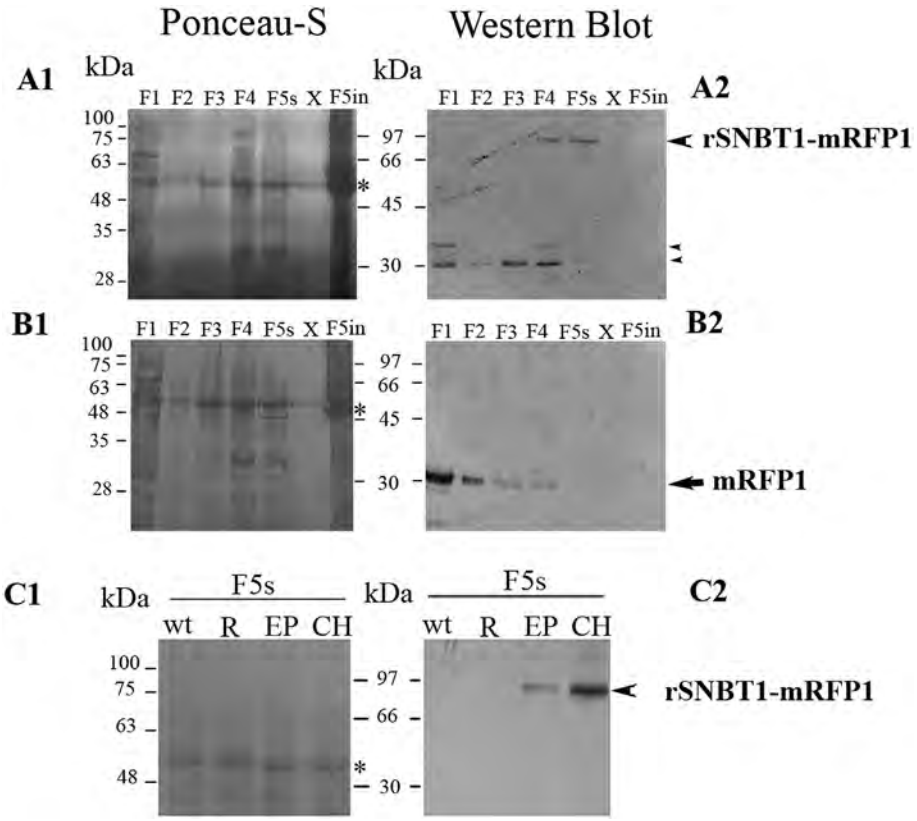

Fig. 4. Biochemical detection of rSNTB1-mRFP1 in transgenic *L. tarentolae-rsnbt1-mrfp1* strains. Western blot analysis was performed on subcellular protein fractions obtained from stationary phase promastigotes of (A) *L. tarentolae-rsnbt1-mrfp1*-CH, (B) *L. tarentolae-mrfp1*or (C) *L. tarentolae-rsnbt1-mrfp1*-EP (EP), *L. tarentolae-rsnbt1-mrfp1*–CH (CH), *L. tarentolae*-wt (wt) and *L. tarentolae-mrfp1* (R) obtained by digitonin fractionation and a further treatment of the final pellet fraction (F5) with 2% v/v Triton X-100 (see *Methods*). In A1, A2, B1 and B2, all fractions F1-F5in were analyzed. In C1 and C2 only the F5s fractions from the 3 recombinant strains and the wt parental line were analyzed. Protein samples were analyzed by SDS-PAGE (10% w/v) and transferred to nitrocellulose membrane which was further incubated with purified anti-mRFP1 rabbit Ab (0.4 μg/ml) and a second anti-rabbit Ab conjugated to HRP. Protein bands were revealed by ECL. Molecular mass standards (in kDa) are shown. Large arrowheads point to the full length rSNBT1-mRFP1 (B2 and C2) and small arrowheads to its C-terminal proteolytic products (B2). An arrow indicates the migration position of the mRFP1 protein (B2). Asterisks in A1, B1 and C1 indicate the migration position of α and β tubulin. X: empty lane. Ponceau-S stained images of the same membranes are presented as loading indicators in A1, B1 and C1.

calculated molecular mass of 92.1 kDa, and was found to be present in fractions F4 and F5s, enriched in ER and plasma membrane proteins, respectively (Fig. 4, panels A and C). Smaller size bands that could be attributed to proteolytic C-terminal fragments of the rSNBT1-mRFP1 protein were also detected with the anti-mRFP pAb in all fractions except in F5s where these bands were barely detectable (Fig. 4, compare panels A and B). The apparent absence of proteolytic fragments of rSNBT1-mRFP1 in the fraction F5s implies that a significant amount of correctly folded, full length recombinant protein reaches the promastigote plasma membrane.

The mRFP1 protein in the *L. tarentolae-mrfp1* promastigote subcellular fractions was mostly detected (Fig. 4B2) in fractions F1 and F2 containing the soluble proteins. As a confirmation of the specificity of the anti-mRFP antibody, no protein band of higher molecular size was detected in any of the fractions of the *L. tarentolae-mrfp1* strain (Fig. 4B2) or of the *L. tarentolae* wild-type LEXSY strain (Fig. 4C2).

Based on the digitonin fractionation analysis, the *L. tarentolae-rsnbt1-mrfp1*-EP parasites appear to express the chimeric transporter at lower amounts than those produced by the *L. tarentolae-rsnbt1-mrfp1*-CH strain (Fig. 4), a result that is consistent with the confocal microscopy findings (Fig. 2B).

In conclusion, the *L. tarentolae-rsnbt1-mrfp1* transgenic parasite strains express the full length rSNBT1-mRFP1 chimeric protein which is targeted to the ER and the plasma membrane of the promastigotes.

3.4. Analysis of nucleobase transport in the L. tarentolae-rsnbt1-mrfp1-CH promastigotes

Functional transport assays were performed in the transgenic *L. tarentolae-rsnbt1-mrfp1*–CH that express the recombinant rSNBT1-mRFP1 at higher levels relative to *L. tarentolae-rsnbt1-mrfp1*–EP and have a larger population of cells with detectable levels of the transporter at the plasma membrane (Figs. 24). Logarithmically grown *L. tarentolae-rsnbt1-mrfp1*–CH promastigotes were assayed for active transport of uracil, hypoxanthine, xanthine and thymine, that are known substrates of rSNBT1 [17], in the presence or absence of putative inhibitors or non-radiolabeled nucleobases as putative competitors. Control *L. tarentolae-mrfp1* and *L. tarentolae* wild-type promastigotes at the logarithmic phase of growth were assayed in parallel, in all cases, to determine the extent of contribution of endogenous transport activities from the *Leishmania* intrinsic nucleobase/nucleoside transporters. *Leishmania* and *Trypanosomatideae* in general lack transporter homologs of family NAT/NCS2 or other nucleobase transporter families [30,32], but they possess nucleoside transporters of the ENT (Equilibrative Nucleoside Transporter) family that are known to transport also free nucleobases [52–57].

As shown in Fig. 5(A–E), *L. tarentolae-rsnbt1-mrfp1*–CH can transport [^{3}H]-uracil, as well as [^{3}H]-xanthine and [^{3}H]-hypoxanthine, but did not show detectable transport of [^{14}C]-thymine (Fig. 5D) at the conditions employed. The transport of [^{3}H]-uracil was linear within the first 5 min of reaction (Fig. 5A) and the uracil transport rate (measured at 1–5 min) was found not to change significantly in the absence of Na^+ (replacement of NaCl in the uptake buffer by choline chloride) (Fig. 5B). Although not shown, the transport rate increased almost linearly with increasing concentrations of [^{3}H]-uracil from 20 nM to 1 μM, implying that the K_M for this substrate should be much higher than 1 μM. The uracil uptake activity was inhibited to a significant extent by dipyridamole, a well-known inhibitor of human ENT transporter [1,58] that also inhibits protozoan ENTs [52] and, with very low apparent affinity, rSNBT1 [17] (Fig. 5C). Despite the ability to transport both xanthine and hypoxanthine (Fig. 5D), the uracil uptake activity of *L.tarentolae-rsnbt1-mrfp1*–CH was inhibited by only about 30–40% in the presence of a 1000-fold molar excess of these purines (Fig. 5E). Finally, the toxic uracil analog 5-fluorouracil (5-FU), which is known to be highly toxic to other *Leishmania* species [53], was found to inhibit the growth of *L. tarentolae-rsnbt1-mrfp1*–CH dramatically, whereas the xanthine analog oxypurinol had no effect on growth (Fig. 5F). Similar results were obtained in all cases with the *L.tarentolae-mrfp1*and wild-type LEXSY controls (Fig. 5F and data not shown).

Overall, the above data indicate that the bulk of nucleobase

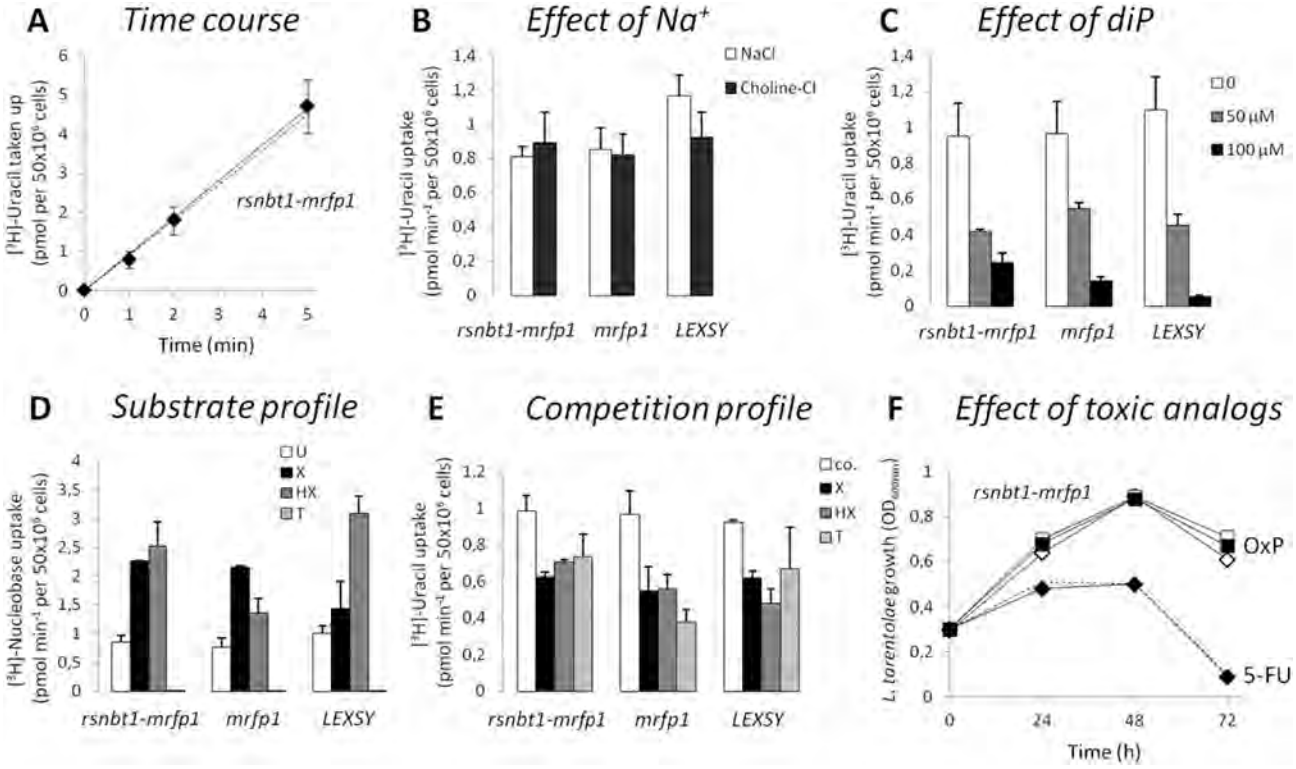

Fig. 5. Nucleobase uptake properties of *L. tarentolae*(*LEXSY*) and transgenic*L.tarentolae-rsnbt1-mrfp1*–CH (*rsnbt1-mrfp1*) and*L.tarentolae-mrfp1*control (*mrfp1*). All *L. tarentolae* cells were cultured in LEXSY Broth BHI with appropriate supplements, in the presence of nourseothricin (1 μg/ml). Wild-type or transgenic LEXSY were harvested at the logarithmic phase of growth and 50 × 10^6 cells/reaction were assayed for uptake of [^{3}H]-uracil (1 μM) (A-E), [^{3}H]-xanthine (1 μM) (D), [^{3}H]-hypoxanthine (1 μM) (D) or [^{14}C]-thymine (10 μM) (D). The transport assays were performed in the presence of 140 mM NaCl, unless otherwise indicated. The values shown in A-E represent the means of three to five measurements with standard deviations given as *error bars*. (A). Time course of the uracil uptake reaction for *rsnbt1-mrfp1*. Very similar data were obtained with *mrfp1* (interrupted line) and LEXSY (not shown). (B). Uracil uptake rates in uptake buffer containing 140 mM NaCl (white bars) or 140 mM choline chloride (black bars). (C). Uracil uptake rates in the absence (white bars) or presence of 50 μM (gray bars) or 100 μM (black bars) of dipyridamole (diP). (D). Uptake rates of uracil (U, white bars), xanthine (X, black bars), hypoxanthine (HX, gray bars), and thymine (T, light gray). (E). Uracil uptake rates in the presence of 1000-fold molar excess (1 mM) of xanthine (X, black bars), hypoxanthine (HX, gray bars) or thymine (T, light gray bars). (F). Cell growth of *rsnbt1-mrfp1* (starting culture, 10^6 cells/ml) in the presence of 0.1 mM of 5-fluorouracil (5-FU, black rhombuses) or 0.1 mM of oxypurinol (OxP, black rectangles); the data for control cells grown in parallel in the absence of 5-FU or OxP are shown in open symbols (rhombuses or rectangles, respectively). Very similar data were obtained with *mrfp1* (interrupted line for growth with 5-FU) and LEXSY (not shown).

transport activity detected in *L. tarentolae-rsnbt1-mrfp1*–CH was due to endogenous ENT transporters of *Leishmania*. The strongest indication comes from the experiment with choline chloride (Fig. 5B), showing no detectable dependence of the uracil uptake on Na^+, a property that points to the properties of *Leishmania* ENT nucleoside/nucleobase transporters which are H^+-dependent, Na^+-independent electrogenic transporters [52,55] and not to the Na^+-dependent rSNBT1 [17]. In addition, thymine which is a known high-affinity substrate of rSNBT1 [17] but not reported as a substrate for any intrinsic *Leishmania* transporter [53–57] was not transported significantly by *L. tarentolae-rsnbt1-mrfp1*–CH (Fig. 5D). The modest inhibition of the [^{3}H]-uracil transport by non-radiolabeled nucleobases (Fig. 5E) is also attributable to endogenous nucleoside/nucleobase-transport activities. Dipyridamole which inhibits the *L. tarentolae-rsnbt1-mrfp1*–CH uracil transport activity significantly (Fig. 5C) is also a potent inhibitor of ENT transporters [52,58]. However, *L. tarentolae-rsnbt1-mrfp1*–CH is less sensitive to dipyridamole than *L. tarentolae-mrfp1*or wild-type LEXSY (Fig. 5C; 100 μM), a property that might be attributed to a fraction of activity related to the exogenously expressed rSNBT1. In consistence with this interpretation, when the cells are incubated with dipyridamole in the absence of Na^+ to exclude the contribution of any exogenous rSNBT1, the residual uracil uptake activity of *L. tarentolae-rsnbt1-mrfp1*–CH decreases to an essentially background level approximating the uptake levels of similarly treated *L. tarentolae-mrfp1* or wild-type LEXSY (Fig. 6).

4. Conclusion/perspectives

We have used *Leishmania tarentolae* for heterologous recombinant expression of a mammalian solute carrier, namely the sodium-nucleobase transporter rSNBT1 of the NAT/NCS2 family (Slc23A.4), and shown that rSNBT1 is targeted to the ER and the plasma membrane of the protozoan promastigotes. Our study is one of the few reports in the literature for expression of a multiple spanning membrane mammalian protein in the *L.tarentolae* system [11,14,15] and the first one for expression of a mammalian solute carrier in this system. Targeting of the rSNBT1-mRFP1 protein to the plasma membrane and the ER of the promastigotes (Figs. 3–4 and S3–S5) was achieved without adding a membrane-targeting/retention signal sequence specific for *Trypanosomatideae* [59,60], indicating that *L.tarentolae* can recognize and process the relevant signals in the sequence of the mammalian solute carrier. Similarly, *Leishmania* surface membrane proteins can be exogenously expressed in the plasma membrane of mammalian cells [40], indicating the compatibility of these organisms in protein sorting and targeting mechanisms. In conjunction with a previous study showing that *L. tarentolae* cell-free extracts can be used for synthesis of correctly folded human solute carriers [61], our current evidence suggests that the convenient and cost-effective *L. tarentolae* system might be an advantageous host for expression/purification and structure-functional analysis of mammalian solute carriers. We also present a quick and direct way to assay biochemically the subcellular distribution of the

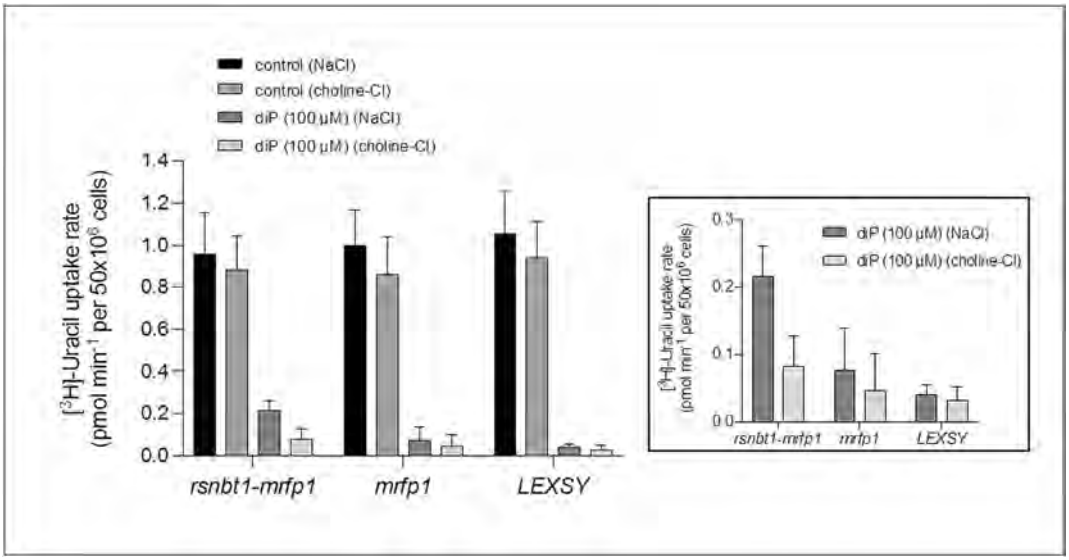

Fig. 6. Effect of dipyridamole on the uracil uptake activities of *L. tarentolae* (*LEXSY*) and transgenic *L. tarentolae-rsnbt1-mrfp1*–CH (*rsnbt1-mrfp1*) and*L.tarentolae-mrfp1*control (*mrfp1*) and its dependence on Na^+ ions. All *L. tarentolae* cells were cultured in LEXSY Broth BHI with appropriate supplements, in the presence of nourseothricin (1 μg/ml). Wild-type or transgenic LEXSY were harvested at the logarithmic phase of growth and 50 × 10^6 cells/reaction were assayed for uptake of [^{3}H]-uracil (1 μM) in uptake buffer containing 140 mM NaCl or 140 mM choline chloride, in the absence or presence of 100 μM dipyridamole (diP), as indicated. The values shown represent the means of three to five measurements with standard deviations given as *error bars*. The data obtained in the presence of diP are also shown on a larger scale at the right side as an *inset*. Unpaired *t*-tests (GraphPad Prism 8.0) indicate statistically significant difference of the residual diP-resistant activity (in Na^+-containing buffer) of *rsnbt1-mrfp1* from its diP-resistant activity in choline-containing buffer (p = 0.0104) or the diP-resistant activity of *mrfp1* or LEXSY in either Na^+-containing or choline-containing buffer (p values ranging from 0.0103 to < 0.0001) (when comparing all six samples by one-way ANOVA, p = 0.0003), whereas the diP-resistant activity of *rsnbt1-mrfp1* in choline-containing buffer does not differ significantly from the diP-resistant activity of *mrfp1* or LEXSY in either Na^+-containing or choline-containing buffer (p values ranging from 0.8952 to 0.0899; comparing all five samples by one-way ANOVA, p = 0.3043).

recombinant membrane protein expressed in *L. tarentolae* by a stepwise subcellular fractionation with digitonin and Triton-X. This approach could be used as a first evaluation step to obtain a fraction enriched in the recombinant protein for further isolation and crystallization attempts.

The transport analysis of the *L.tarentolae* promastigotes expressing rSNBT1-mRFP1 indicates that most of the purine-pyrimidine uptake activity in the transgenic parasites is probably due to endogenous transport systems of the host (Fig. 5). The genome of *L. tarentolae* contains four nucleoside/nucleobase transporter homologs, two of which are probably present at the promastigote stage and may contribute to the observed nucleobase transport properties, based on functional evidence for their counterparts in other *Leishmania* species (Supplemental Table S1). More specifically, *L. tarentolae* NT1.1 (UUT1) [53] could be responsible for the transport of uracil and the sensitivity to 5-FU whereas *L.tarentolae* NT3 [62] could be responsible for the transport of xanthine and hypoxanthine (Table S1 and Fig. 5). The contribution of the transport activity of the exogenously expressed rSNBT1 appears to be negligible or very limited because specific properties of rSNBT1 that could differentiate it from the endogenous activity (dependence on Na^+, transport of thymine, insensitivity to dipyridamole) [17,63] (Table S2) are not detectable in the assays (Fig. 5). Nevertheless, the residual dipyridamole-resistant activity of the transgenic *L.tarentolae-rsnbt1-mrfp1*–CH is dependent on Na^+ ions, implying that this fraction of activity is due to the heterologously expressed rSNBT1 (Fig. 6). The possibility that rSNBT1 is not present at sufficient quantities in the plasma membrane of the promastigote cells cannot be ruled out. However, the colocalization results (Figs. 3B, S5 and S6) obtained from the quantitative image analysis of the microscopy data and the digitonin fractionation data (Fig. 4) imply that a significant amount of the recombinant full-length transporter reaches the plasma membrane, although a large fraction seems to localize intracellularly, in the ER, as expected. It is also improbable that the C-terminally fused mRFP1 protein affects the transport activity to a major extent, since GFP-tagged rSNBT1 was shown to be active for uracil transport in MDCKII cells [17] and C-terminally GFP-tagged versions of several bacterial [64], fungal [65] and mammalian [37,38] homologs of rSNBT1 were also shown to be active in various systems. In view of all the above evidence, the issue of functionality of the expressed rSNBT1-mRFP1 transporter could be resolved further in future work with chromosomal inactivation of the appropriate endogenous ENT of *L. tarentolae* (Table S1) and attempts to complement functionally with the heterologous expression of rSNBT1.

Supplementary data to this article can be found online at https://doi.org/10.1016/j.bbamem.2019.07.001.

Acknowledgments

Microscopy work was performed in the Light Microscopy unit of the Hellenic Pasteur Institute (HPI-LMU).

Author contribution

Conceived and designed the experiments: HB and SF. Performed the experiments: AD, EK, MB, KP, AP, OT. Analyzed the data: AD, EX, HB, and SF. Contributed reagents/materials/analysis tools: HB and SF. Wrote the paper: AD, HB and SF.

Funding

1) This research has been co-financed by the European Union (European Social Fund – ESF) and Greek national funds through the Operational Program “Education and Lifelong Learning” of the National Strategic Reference Framework (NSRF) – Research Funding Program: THALES, Investing in knowledge society through the European Social Fund and 2) by the Greek GSRT's KRIPIS II action, co-financed by \Greek national funds and the European Union (European Regional Development Fund) NSRF 2014–2020 (MIS 5002486), Operational

programme Competitiveness, Research and Innovation.

Declaration of Competing Interest

The funders had no role in study design, data collection and analysis, decision to publish, or preparation of the manuscript.

References

[1] A. César-Razquin, B. Snijder, T. Frappier-Brinton, R. Isserlin, G. Gyimesi, X. Bai, R.A. Reithmeier, D. Hepworth, M.A. Hediger, A.M. Edwards, G. Superti-Furga, A call for systematic research on Solute Carriers, Cell 62 (2015) 478–487, https://doi.org/10.1016/j.cell.2015.07.022.

[2] Y. He, K. Wang, N. Yan, The recombinant expression systems for structure determination of eukaryotic membrane proteins, Protein Cell 5 (2014) 658–672, https://doi.org/10.1007/s13238-014-0086-4.

[3] T.D. Newport, M.S.P. Sansom, P.J. Stansfeld, The MemProtMD database: a resource for membrane-embedded protein structures and their lipid interactions, Nucleic Acids Res. 47 (2019) D390–D397, https://doi.org/10.1093/nar/gky1047.

[4] R. Breitling, S. Klinger, N. Callewert, R. Pietrucha, A. Geyer, G. Ehrlich, P. Hartung, A. Müller, R. Contreras, S.M. Beverley, K. Alexandrov, Non-pathogenic trypanosomatid protozoa as a platform for protein research and production, Protein Expr. Purif. 25 (2002) 209–218, https://doi.org/10.1016/S1046-5928(02)00001-3.

[5] L. Simpson, G. Holz Jr., The status of *Leishmania tarentolae/Trypanosoma platydactyli*, Parasitol. Today 4 (1988) 115–118, https://doi.org/10.1016/0169-4758(88)90043-9.

[6] S. Coughlan, P. Mulhair, M. Sanders, G. Schonian, J.A. Cotton, T. Downing, The genome of *Leishmania adleri* from a mammalian host highlights chromosome fission in Sauroleishmania, Sci. Rep. 7 (2017) 43747, , https://doi.org/10.1038/srep43747.

[7] F. Raymond, S. Boisvert, G. Roy, J.F. Ritt, D. Légaré, A. Isnard, M. Stanke, M. Olivier, M.J. Tremblay, B. Papadopoulou, M. Ouellette, J. Corbell, Genome sequencing of the lizard parasite *Leishmania tarentolae* reveals loss of genes associated to the intracellular stage of human pathogenic species, Nucleic Acids Res. 40 (2012) 1131–1147, https://doi.org/10.1093/nar/gkr834.

[8] G. Basile, M. Peticca, Recombinant protein expression in *Leishmania tarentolae*, Mol. Biotechnol. 43 (2009) 273–278, https://doi.org/10.1007/s12033-009-9213-5.

[9] T. Niimi, Recombinant protein production in the eukaryotic protozoan parasite *Leishmania tarentolae*: a review, Methods Mol. Biol. 824 (2012) 307–315, https://doi.org/10.1007/978-1-61779-433-9_15.

[10] A.H. Khan, H. Bayat, M. Rajabibazi, S. Sabri, A. Rahimpour, Humanizing glycosylation pathways in eukaryotic expression systems, World J. Microbiol. Biotechnol. 33 (2017) 4, , https://doi.org/10.1007/s11274-016-2172-7.

[11] T. Langer, C. Corvey, K. Kroll, O. Boscheinen, T. Wendrich, W. Dittrich, Expression and purification of the extracellular domains of human glycoprotein VI (GPVI) and the receptor for advanced glycation end products (RAGE) from *Rattus norvegicus* in *Leishmania tarentolae*, Prep. Biochem. Biotechnol. 47 (2017) 1008–1015, https://doi.org/10.1080/10826068.2017.1365252.

[12] S. Foldynova-Trantirkova, J. Matulova, V. Dötsch, F. Löhr, I. Cirstea, K. Alexandrov, R. Breitling, J. Lukes, L. Trantirek, A cost-effective amino-acid-type selective isotope labeling of proteins expressed in *Leishmania tarentolae*, J. Biomol. Struct. Dyn. 26 (2009) 755–761, https://doi.org/10.1080/07391102.2009.10507287.

[13] A. Niculae, P. Bayer, I. Cirstea, T. Bergbrede, R. Pietrucha, M. Gruen, R. Breitling, K. Alexandrov, Isotopic labeling of recombinant proteins expressed in the protozoan host *Leishmania tarentolae*, Protein Expr. Purif. 48 (2006) 167–172, https://doi.org/10.1016/j.pep.2006.04.006.

[14] L. Gonzalez-Lobato, V. Chaptal, J. Molle, P. Falson, *Leishmania tarentolae* as a promising tool for expressing polytopic and multi-transmembrane spans eukaryotic membrane proteins: the case of the ABC pump ABCG6, Methods Mol. Biol. 1432 (2016) 119–131, https://doi.org/10.1007/978-1-4939-3637-3_8.

[15] J. Grebowski, M. Studzian, G. Bartosz, L. Pulaski, *Leishmania tarentolae* as a host for heterologous expression of functional human ABCB6 transporter, Biochim. Biophys. Acta, Biomembr. 1858 (2016) 2617–2624, https://doi.org/10.1016/j.bbamem.2016.06.022.

[16] O. Volkov, K. Kovalev, V. Polovinkin, V. Borshchevskiy, C. Bamann, R. Astashkin, E. Marin, A. Popov, T. Balandin, D. Willbold, G. Büldt, E. Bamberg, V. Gordeliy, Structural insights into ion conduction by channelrhodopsin 2, Science 358 (2017) eaan8862, https://doi.org/10.1126/science.aan8862.

[17] S. Yamamoto, K. Inoue, T. Murata, S. Kamigaso, T. Yasujima, J. Maeda, Y. Yoshida, K. Ohta, H. Yuasa, Identification and functional characterization of the first nucleobase transporter in mammals: implication in the species difference in the intestinal absorption mechanism of nucleobases and their analogs between higher primates and other mammals, J. Biol. Chem. 285 (2010) 6522–6531, https://doi.org/10.1074/jbc.M109.032961.

[18] A. Chaliotis, P. Vlastaridis, C. Ntountoumi, M. Botou, V. Yalelis, P. Lazou, E. Tatsaki, D. Mossialos, S. Frillingos, G.D. Amoutzias, NAT/NCS2-hound: a webserver for the detection and evolutionary classification of prokaryotic and eukaryotic nucleobase-cation symporters of the NAT/NCS2 family, GigaScience 7 (2018) giy133, https://doi.org/10.1093/gigascience/giy133.

[19] M.H. Saier Jr., V.S. Reddy, B.V. Tsu, M.S. Ahmed, C. Li, G. Moreno-Hagelsieb, The Transporter Classification Database (TCDB): recent advances, Nucleic Acids Res. 44 (2016) D372–D379, https://doi.org/10.1093/nar/gkv1103.

[20] Y. Alguel, S. Amillis, J. Leung, G. Lambrinidis, S. Capaldi, N.J. Scull, G. Craven, S. Iwata, A. Armstrong, E. Mikros, G. Diallinas, A.D. Cameron, B. Byrne, Structure of eukaryotic purine/H(+) symporter UapA suggests a role for homodimerization in transport activity, Nat. Commun. 7 (2016) 11336, , https://doi.org/10.1038/ncomms11336.

[21] T. Arakawa, T. Kobayashi-Yurugi, Y. Alguel, H. Iwanari, H. Hatae, M. Iwata, Y. Abe, T. Hino, C. Ikeda-Suno, H. Kuma, D. Kang, T. Murata, T. Hamakubo, A.D. Cameron, T. Kobayashi, N. Hamasaki, S. Iwata, Crystal structure of the anion exchanger domain of human erythrocyte band 3, Science 350 (2015) 680–684, https://doi.org/10.1126/science.aaa4335.

[22] Y.N. Chang, E.R. Geertsma, The novel class of seven transmembrane segment inverted repeat carriers, Biol. Chem. 398 (2017) 165–174, https://doi.org/10.1515/hsz-2016-0254.

[23] E.R. Geertsma, Y.N. Chang, F.R. Shaik, Y. Neldner, E. Pardon, J. Steyaert, R. Dutzler, Structure of a prokaryotic fumarate transporter reveals the architecture of the SLC26 family, Nat. Struct. Mol. Biol. 22 (2015) 803–808, https://doi.org/10.1038/nsmb.3091.

[24] K.W. Huynh, J. Jiang, N. Abuladze, K. Tsirulnikov, L. Kao, X. Shao, D. Newman, R. Azimov, A. Pushkin, Z.H. Zhou, I. Kurtz, CryoEM structure of the human SLC4A4 sodium-coupled acid-base transporter NBCe1, Nat. Commun. 9 (2018) 900, , https://doi.org/10.1038/s41467-018-03271-3.

[25] F. Lu, S. Li, Y. Jiang, J. Jiang, H. Fan, G. Lu, D. Deng, S. Dang, X. Zhang, J. Wang, N. Yan, Structure and mechanism of the uracil transporter UraA, Nature 472 (2011) 243–246, https://doi.org/10.1038/nature09885.

[26] B.H. Thurtle-Schmidt, R.M. Stroud, Structure of Bor1 supports an elevator transport mechanism for SLC4 anion exchangers, Proc. Natl. Acad. Sci. U. S. A. 113 (2016) 10542–10546, https://doi.org/10.1073/pnas.1612603113.

[27] X. Yu, G. Yang, C. Yan, J.L. Baylon, J. Jiang, H. Fan, G. Lu, K. Hasegawa, H. Okumura, T. Wang, E. Tajkhorshid, S. Li, N. Yan, Dimeric structure of the uracil:proton symporter UraA provides mechanistic insights into the SLC4/23/26 transporters, Cell Res. 27 (2017) 1020–1033, https://doi.org/10.1038/cr.2017.83.

[28] M. Botou, P. Lazou, K. Papakostas, G. Lambrinidis, T. Evangelidis, E. Mikros, S. Frillingos, Insight on specificity of uracil permeases of the NAT/NCS2 family from analysis of the transporter encoded in the pyrimidine utilization operon of *Escherichia coli*, Mol. Microbiol. 108 (2018) 204–219, https://doi.org/10.1111/mmi.13931.

[29] M. Bürzle, Y. Suzuki, D. Ackermann, H. Miyazaki, N. Maeda, B. Clémençon, R. Burrier, M.A. Hediger, The sodium-dependent ascorbic acid transporter family SLC23, Mol. Asp. Med. 34 (2013) 436–454, https://doi.org/10.1016/j.mam.2012.12.002.

[30] S. Frillingos, Insights to the evolution of Nucleobase-Ascorbate Transporters (NAT/NCS2 family) from the Cys-scanning analysis of xanthine permease XanQ, Int J Biochem Mol Biol 3 (2012) 250–272 https://www.ncbi.nlm.nih.gov/pmc/articles/PMC3476789/.

[31] C. Girke, N. Daumann, S. Niopek-Witz, T. Möhlmann, Nucleobase and nucleoside transport and integration into plant metabolism, Front. Plant Sci. 5 (2014) 443, , https://doi.org/10.3389/fpls.2014.00443.

[32] C. Gournas, I. Papageorgiou, G. Diallinas, The nucleobase-ascorbate transporter (NAT) family: genomics, evolution, structure-function relationships and physiological role, Mol. BioSyst. 4 (2008) 404–416, https://doi.org/10.1039/b719777b.

[33] E. Karena, E. Tatsaki, G. Lambrinidis, E. Mikros, S. Frillingos, Analysis of conserved NCS2 motifs in the *Escherichia coli* xanthine permease XanQ, Mol. Microbiol. 98 (2015) 502–517, https://doi.org/10.1111/mmi.13138.

[34] A. Kourkoulou, A.A. Pittis, G. Diallinas, Evolution of substrate specificity in the Nucleobase-Ascorbate Transporter (NAT) protein family, Microb. Cell 5 (2018) 280–292, https://doi.org/10.15698/mic2018.06.636.

[35] S. Sotiriou, S. Gispert, J. Cheng, Y. Wang, A. Chen, S. Hoogstraten-Miller, G.F. Miller, O. Kwon, M. Levine, S.H. Guttentag, R.L. Nussbaum, Ascorbic-acid transporter Slc23a1 is essential for vitamin C transport into the brain and for perinatal survival, Nat. Med. 8 (2002) 514–517, https://doi.org/10.1038/nm0502-514.

[36] H. Tsukaguchi, T. Tokui, B. Mackenzie, U.V. Berger, X.Z. Chen, Y. Wang, R.F. Brubaker, M.A. Hediger, A family of mammalian Na^+-dependent L-ascorbic acid transporters, Nature 399 (1999) 70–75, https://doi.org/10.1038/19986.

[37] V. Ormazabal, F.A. Zuniga, E. Escobar, C. Aylwin, A. Salas-Burgos, A. Godoy, A.M. Reyes, J.C. Vera, C.I. Rivas, Histidine residues in the Na^+-coupled ascorbic acid transporter-2 (SVCT2) are central regulators of SVCT2 function, modulating pH sensitivity, transporter kinetics, Na^+ cooperativity, conformational stability, and subcellular localization, J. Biol. Chem. 2010 (285) (2010) 36471–36485, https://doi.org/10.1074/jbc.M110.155630.

[38] S. Varma, C.E. Campbell, S.M. Kuo, Functional role of conserved transmembrane segment 1 residues in human sodium-dependent vitamin C transporters, Biochemistry 47 (2008) 2952–2960, https://doi.org/10.1021/bi701666q.

[39] V.S. Subramanian, J.S. Marchant, J.C. Reidling, H.M. Said, N-glycosylation is required for Na^+-dependent vitamin C transporter functionality, Biochem. Biophys. Res. Commun. 374 (2008) 123–127, https://doi.org/10.1016/j.bbrc.2008.06.120.

[40] A.M. Velho, S.M. Jarvis, Topological studies of hSVCT1, the human sodium-dependent vitamin C transporter and the influence of N-glycosylation on its intracellular targeting, Exp. Cell Res. 315 (2009) 2312–2321, https://doi.org/10.1016/j.yexcr.2009.04.007.

[41] A. Papadaki, A.S. Politou, D. Smirlis, M.P. Kotini, K. Kourou, T. Papamarcaki, H. Boleti, The *Leishmania donovani* histidine acid ecto-phosphatase LdMAcP: insight into its structure and function, Biochem. J. 467 (2015) 473–486, https://doi.org/10.1042/BJ20141371.

[42] A.L. Foucher, B. Papadopoulou, M. Ouellette, Prefractionation by digitonin extraction increases representation of the cytosolic and intracellular proteome of *Leishmania infantum*, J. Proteome Res. 5 (2006) 1741–1750, https://doi.org/10.

1021/pr060081j.
[43] U.K. Laemmli, Cleavage of structural proteins during the assembly of the head of bacteriophage T4, Nature 227 (1970) 680–685, https://doi.org/10.1038/227680a0.
[44] C.A. Schneider, W.S. Rasband, K.W. Eliceiri, NIH image to ImageJ: 25 years of image analysis, Nat. Methods 9 (2012) 671–675, https://doi.org/10.1038/nmeth.2089.
[45] J.D. Bangs, L. Uyetake, M.J. Brickman, A.E. Balber, J.C. Boothroyd, Molecular cloning and cellular localization of a BiP homologue in *Trypanosoma brucei*. Divergent ER retention signals in a lower eukaryote, J. Cell Sci. 105 (1993) 1101–1113 https://www.ncbi.nlm.nih.gov/pubmed/8227199.
[46] S.V. Costes, D. Daelemans, E.H. Cho, Z. Dobbin, G. Pavlakis, S. Lockett, Automatic and quantitative measurement of protein-protein colocalization in live cells, Biophys. J. 86 (2004) 3993–4003, https://doi.org/10.1529/biophysj.103.038422.
[47] S. Kumar, G. Stecher, K. Tamura, MEGA7: Molecular Evolutionary Genetics Analysis version 7.0 for bigger datasets, Mol. Biol. Evol. 33 (2016) 1870–1874, https://doi.org/10.1093/molbev/msw054.
[48] M. Aslett, C. Aurrecoechea, M. Barriman, J. Brestelli, B.P. Brunk, M. Carrington, D.P. Depledge, S. Fischer, B. Gajria, X. Gao, M.J. Gardner, A. Gingle, G. Grant, O.S. Harb, M. Heiges, C. Hertz-Fowler, R. Houston, F. Innamorato, J. Iodice, J.C. Kissinger, E. Kraemer, W. Li, F.J. Logan, J.A. Miller, P.J. Myler, V. Nayak, C. Pennington, I. Phan, D.F. Pinney, G. Ramasamy, M.B. Rogers, D.S. Roos, C. Ross, D. Sivam, D.F. Smith, G. Srinivasamoorthy, C.J. Stoeckert Jr., S. Subramanian, R. Thibodeau, A. Tivey, C. Treatman, G. Velarde, H. Wang, TriTrypDB: a functional genomic resource for the Trypanosomatidae, Nucleic Acids Res. 38 (2010) D457–D462, https://doi.org/10.1093/nar/gkp851.
[49] S. Bienert, A. Waterhouse, T.A. de Beer, G. Tauriello, G. Studer, L. Bordoli, T. Schwede, The SWISS-MODEL repository-new features and functionality, Nucleic Acids Res. 45 (2017) D313–D319, https://doi.org/10.1093/nar/gkw1132.
[50] W. de Souza, M. Attias, Subpellicular microtubules in Apicomplexa and Trypanosomatids, in: W. de Souza (Ed.), Structures and Organelles in Pathogenic Protists. Microbiology Monographs, 17 Springer, Berlin, Heidelberg, 2010, pp. 27–62, , https://doi.org/10.1007/978-3-642-12863-9_2.
[51] P.F. Pimenta, W. de Souza, Fine structure and cytochemistry of the endoplasmic reticulum and its association with the plasma membrane of *Leishmania mexicana amazonensis*, J. Submicrosc. Cytol. 17 (1985) 413–419 https://www.ncbi.nlm.nih.gov/pubmed/4020925.
[52] S.M. Landfear, B. Ullman, N.S. Carter, M.A. Sanchez, Nucleoside and nucleobase transporters in parasitic protozoa, Eukaryot. Cell 3 (2004) 245–254, https://doi.org/10.1128/ec.3.2.245-254.2004.
[53] K.J.H. Alzahrani, J.A.M. Ali, A.A. Eze, W.L. Looi, D.N.A. Tagoe, D.J. Creek, M.P. Barrett, H.P. de Koning, Functional and genetic evidence that nucleoside transport is highly conserved in *Leishmania* species: implications for pyrimidine-based chemotherapy, Int. J. Parasitol. Drugs Drug Resist. 7 (2017) 206–226, https://doi.org/10.1016/j.ijpddr.2017.04.003.
[54] N.S. Carter, P.A. Yates, S.K. Gessford, S.R. Galagan, S.M. Landfear, B. Ullman, Adaptive responses to purine starvation in *Leishmania donovani*, Mol. Microbiol. 78 (2010) 92–107, https://doi.org/10.1111/j.1365-2958.2010.07327.x.
[55] H.P. de Koning, D.J. Bridges, R.J. Burchmore, Purine and pyrimidine transport in pathogenic protozoa: from biology to therapy, FEMS Microbiol. Rev. 29 (2005) 987–1020, https://doi.org/10.1016/j.femsre.2005.03.004.
[56] D. Ortiz, R. Valdés, M.A. Sanchez, J. Hayenga, C. Elya, S. Detke, S.M. Landfear, Purine restriction induces pronounced translational upregulation of the NT1 adenosine/pyrimidine nucleoside transporter in *Leishmania major*, Mol. Microbiol. 78 (2010) 108–118, https://doi.org/10.1111/j.1365-2958.2010.07328.x.
[57] I.G. Papageorgiou, L. Yakob, M.I. Al Salabi, G. Diallinas, K.P. Soteriadou, H.P. de Koning, Identification of the first pyrimidine nucleobase transporter in *Leishmania*: similarities with the *Trypanosoma brucei* U1 transporter and antileishmanial activity of uracil analogues, Parasitology 130 (2005) 275–283 https://www.ncbi.nlm.nih.gov/pubmed/15796010.
[58] R.C. Boswell-Casteel, F.A. Hays, Equilibrative nucleoside transporters-a review, Nucleosides Nucleotides Nucleic Acids 36 (2017) 7–30, https://doi.org/10.1080/15257770.2016.1210805.
[59] C. Clayton, T. Häusler, J. Blattner, Protein trafficking in kinetoplastid protozoa, Microbiol. Rev. 59 (1995) 325–344 https://www.ncbi.nlm.nih.gov/pmc/articles/PMC239364/.
[60] X. Qiao, B.F. Chuang, Y. Jin, M. Muranjan, C.H. Hung, P.T. Lee, M.G. Lee, Sorting signals required for trafficking of the cysteine-rich acidic repetitive transmembrane protein in *Trypanosoma brucei*, Eukaryot. Cell 5 (2006) 1229–1242, https://doi.org/10.1128/EC.00064-06.
[61] S. Ruehrer, H. Michel, Exploiting *Leishmania tarentolae* cell-free extracts for the synthesis of human solute carriers, Mol. Membr. Biol. 30 (2013) 288–302, https://doi.org/10.3109/09687688.2013.807362.
[62] M.A. Sanchez, R. Tryon, S. Pierce, G. Vasudevan, S.M. Landfear, Functional expression and characterization of a purine nucleobase transporter gene from *Leishmania major*, Mol. Membr. Biol. 21 (2004) 11–18, https://doi.org/10.1080/0968768031000140845.
[63] T. Yasujima, C. Murata, Y. Mimura, T. Murata, M. Ohkubo, K. Ohta, K. Inoue, H. Yuasa, Urate transport function of rat sodium-dependent nucleobase transporter 1, Physiol. Rep. 6 (2018) e13714, , https://doi.org/10.14814/phy2.13714.
[64] P. Karatza, S. Frillingos, Cloning and functional characterization of two bacterial members of the NAT/NCS2 family in *Escherichia coli*, Mol. Membr. Biol. 22 (2005) 251–261, https://doi.org/10.1080/09687860500092927.
[65] A. Pantazopoulou, N.D. Lemuh, D.G. Hatzinikolaou, C. Drevet, G. Cecchetto, C. Scazzocchio, G. Diallinas, Differential physiological and developmental expression of the UapA and AzgA purine transporters in *Aspergillus nidulans*, Fungal Genet. Biol. 44 (2007) 627–640, https://doi.org/10.1016/j.fgb.2006.10.003.